

Surface profilometry by a holographic confocal microscopy

RADIM CHMELÍK, LUDĚK LOVICAR, ZDENĚK HARNA

Brno University of Technology, Technická 2, CZ-616 69 Brno, Czech Republic,
e-mail: chmelik@ufi.fme.vutbr.cz.

Confocal imaging by a holographic confocal microscope is based on the real-time incoherent holography. Besides the image amplitude, the image phase is inherently reconstructed. In this paper, we demonstrate that the phase image component can be converted into the height map of the specimen surface, and, in this way, we can measure the surface profile with the precision of several nanometers. The possible ambiguity in the height determination of large height steps is overcome owing to the depth-discrimination property of the microscope. The axial resolution required for this purpose is achieved using broadband illumination.

Keywords: profilometry, confocal microscopy, holographic applications, interferometry.

1. Introduction

A light beam is a convenient probe for the non-destructive measurement of surface profiles. If a specimen surface is imaged by an interference microscopy, the phase shift of the beam is visualised at each point of the surface, and the phase map thus obtained can be converted into the height map. This technique achieves subnanometer resolution [1], but fails partially in the case of high gradients of height (jumps), which can cause ambiguities $m2\pi$ (m is an unknown integer) in the phase map. The height map then contains related ambiguous jumps of the value $m\Delta z$. The integer m can be determined by an independent, less precise, but unambiguous measurement of the height profile of the specimen. A confocal microscopy [2], which enables depth-discriminated microscopic imaging, seems to be the convenient independent optical method for surface measurements. This technique massively suppresses images of defocused regions of a specimen and performs fine optical sections of three-dimensional objects. Thus, the surface profiles of specimens can be reconstructed from a series of optical sections [3].

Conventional confocal and interference microscopes are apparatuses of completely different construction. As the depth discrimination of imaging is usually approached by the dual scanning of a specimen, *i.e.*, by a point source and by a point detector, the optical system of a conventional confocal microscope must contain a scanning system

such as the Nipkow disc or oscillating mirrors [2]. An interference microscope detects the phase component of an image by observing its interference with the reference beam of known parameters. Hence, it usually uses the interferometric system of the Michelson or Mirau type (for the reflected-light observation) or of the Mach–Zehnder type (for the transmitted-light observation).

One can directly combine confocal and interference microscopes and take advantage of simultaneous imaging by the two techniques. The example of such a combination is a confocal interference microscope – a scanning confocal microscope extended by a reference optical branch and an additional detector branch, which was applied in surface profilometry [4]. However, when applying the interference phenomenon to phase detection, it seems convenient to use it also for achieving the confocal (depth-discriminated) imaging, and thus to avoid using any kind of a scanning system. The technique based on this property is known as incoherent holography. The optical system for the incoherent holography is composed of two branches, the object one and the reference one. The light beams outcoming from these two branches interfere in some output (detection) plane of the apparatus. Provided the angle between the beams is non-zero, the spatial carrier is formed in the same way as in the off-axis holography. The intensity and the phase of the image can be reconstructed from the recorded interference structure, if the carrier frequency is at least three times that of the maximum image spatial frequency. This principle, called incoherent holography with spatial carrier, is used by the holographic confocal microscope (HCM) [5]. If the angle is too small or zero, the complete reconstruction of the two image components needs several images recorded with different phase shifts of the reference beam. This technique, incoherent holography with (spatio)temporal carrier, is used, for example, by the microscope with spatiotemporal digital holography [6]. In the two cases, the depth discrimination of the image is achieved by the use of a spatially or spatiotemporally incoherent illumination. Only the light which is scattered at a definite depth of a specimen interferes in the output plane.

The holographic confocal microscope (HCM) is based on the method of incoherent image-plane holography with spatial carrier. It was implemented in the configuration with the Köhler illumination, a reflected-light observation, an electronic real-time detection of the hologram and its on-line digital reconstruction. The microscope uses neither a scanning system nor temporally variable filters. Hence, the image-plane hologram of a single optical section is formed continuously in time and the imaging frequency is limited only by the speed of the camera and of the image-processing procedure.

2. Optical system of the microscope and the image processing

The incoherent light beam generated by an extended source and by the illumination system (Fig. 1) is split into two branches of the microscope by the binary phase grating (150 mm^{-1}). We use a halogen tungsten lamp as the source of polychromatic light, possibly in the combination with the narrow-band filter. The light spot generated on

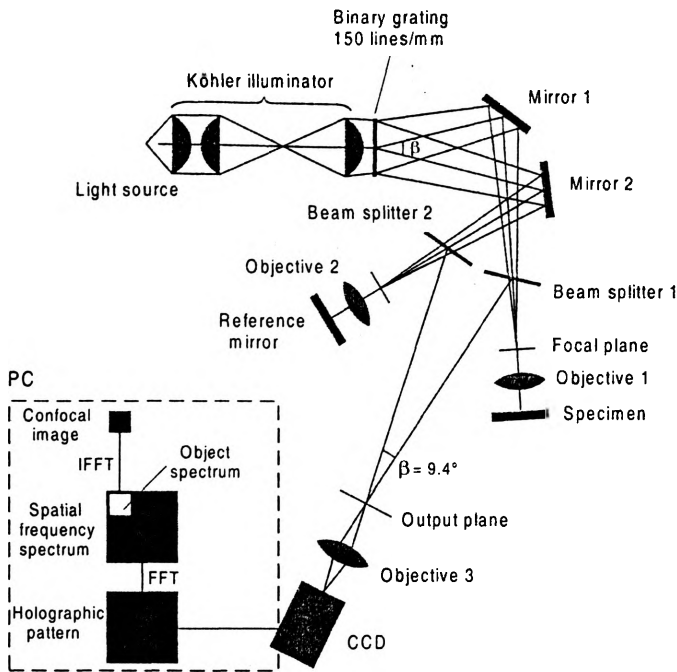


Fig. 1. Optical system of the holographic confocal microscope and image processing.

a rotating diffuser by a He-Ne laser or by a laser diode is used as the monochromatic source. The light beams in individual branches are reflected by the specimen and by the reference mirror and they form images of the two respective objects in the output plane of the microscope by means of objectives 1 and 2. The two beams interfere in the output plane, but, with respect to their spatiotemporal incoherence, the visibility of fringes attains significant values only for the light which is reflected or scattered by the in-focus region of the specimen. Being thus generated, the image-plane hologram of a single optical section of the specimen is detected by the CCD camera and then processed by the computer (see Fig. 1).

First, the two-dimensional Fourier transform is computed by the FFT algorithm. Then, the spatial-frequency spectrum of the object image is obtained by the windowing operation on the sideband of the spatial-frequency spectrum of the hologram. Zero spatial frequency is shifted to the centre of the window and the spectrum is multiplied by the Hanning weight function. Finally, the image complex amplitude is computed by the inverse Fourier transform, and the image phase and the image intensity are separated from it.

3. Principle and experiment

The height-profile measurement requires knowledge of the dependence $\phi(z)$ of the image phase on the defocus z of an image point. The approximation of this dependence

can be derived from axial response $a(z)$ of the microscope for a plane which describes the dependence of complex amplitude a of a planar object image on its distance z from the object plane (defocus). The approximation of the axial response of HCM for low numerical aperture (low-NA) objectives ($NA < 0.5$) has the form [7]

$$a(z) \approx \exp[-2\pi ik(1 + \cos \alpha)z] \operatorname{sinc}[2\pi k(1 - \cos \alpha)z] \quad (1)$$

where $k = 1/\lambda$ denotes the wave number of the illumination in the object space, α is the angular aperture of objectives 1 and 2, and $\operatorname{sinc}x = (\sin x)/x$. In this approximation, the argument of the phasor describes linear dependence of the phase on the defocus

$$\phi(z) \approx -2\pi k(1 + \cos \alpha)z, \quad (2)$$

and the sinc function expresses the depth-discrimination property of the microscope. Evidently, the finesse of the optical section decreases with decreasing aperture α , while the phase sensitivity to the defocus increases.

Equation (2) enables us to convert the phase image component to the height profile of a sample. The most accurate results are obtained from the phase image corresponding to the maximum of the modulus $|a(z)|$, *i.e.*, to the central part of an optical section. The reasons are twofold:

1. Here, the approximation (1) is very close to the correct theoretical formula and the correct phase dependence is linear even for high-NA objectives [7]. The proportionality constant can eventually be precised by the measurement of a calibration sample with defined height change.

2. The statistical r.m.s.-error of the phase measurement caused by the noise is inversely proportional to the fringe visibility [8] and, consequently, inversely proportional to $|a(z)|$. Hence, it has its minimum value for the maximum of $|a(z)|$.

For this reason, the map of a surface with a large height scale should be composed of several optical sections to achieve low rms error of the overall measurement. The distance of adjacent sections is then computed from the phase shift of points inside the sections overlap.

The height map of a surface with large and steep height steps can contain the ambiguity $m\Delta z = -m\lambda/(1 + \cos \alpha)$ resulting from the phase ambiguity $m2\pi$ according to Eq. (2). The unknown integer m can be determined by the independent measurement of the height step taking advantage of the optical sectioning property of HCM and using the profilometric methods developed for a conventional confocal microscopy [3]. In contrast to a conventional confocal microscopy, the required axial resolution of the microscope better than Δz can be achieved without applying high-NA objectives – using a broadband illumination [9].

In this case, the complex-amplitude contributions of different wavelengths are superimposed in the output image [9] and the approximation of the complex-amplitude axial response for low-NA objectives takes the form [7]

$$a(z) \approx \exp[-2\pi i(k_2 + k_1 \cos \alpha)z] \text{sinc}[2\pi(k_2 - k_1 \cos \alpha)z] \quad (3)$$

where k_1, k_2 denote the limits of the spectral band of illumination in the object space. The full width in the half maximum (FWHM) of the modulus of polychromatic response (Eq. (3)) is then in the ratio

$$\frac{k(1 - \cos \alpha)}{k_2 - k_1 \cos \alpha} \quad (4)$$

to the FWHM of the modulus of the monochromatic one described by Eq. (1). The axial resolutions for a broad-band illumination and for a monochromatic one are in the same ratio.

4. Calibration measurement

Several series of images of a high-quality plane mirror have been registered under fixed experimental conditions for different values of $|a|$. The map of unwanted phase shifts introduced by aberrations of the HCM optical system was computed by averaging phase images in a series. Consequently, the unwanted phase shifts were numerically eliminated from the phase images of measured specimens.

An r.m.s.-error estimate of the phase measurement for various values of the amplitude modulus $|a|$ was found from the series. Normal distribution of the phase values at individual image points was proved by the standard χ -square test. On this basis, the r.m.s.-error of the height measurement was estimated from the value of $|a|$ at each image point of the measured specimens.

5. Single-optical-section measurement

The specimen with a linear height step on the surface was prepared by the deposition of a positive polymer photoresist (PMMA) on a glass plane substrate, its exposition by an electron lithography technique and its development in a solver. The silver film was then evaporated on the photoresist surface. The mean depth of the step of about 60 nm was measured by a Talystep stylus profilometer. The specimen surface was then measured by HCM with planachromat objectives Nikon 10 \times /NA = 0.25, and with a laser diode ($\lambda = 659$ nm) illumination. The output signal was captured by a slow-scan cooled digital camera SBIG ST-7.

The height map shown in Fig. 2 was converted from the phase image of the test surface corresponding to the image intensity maximum by means of Eq. (2). It reveals lattice structure in the deeper region of the surface produced during the specimen preparation. The presence of the structure was confirmed by the AFM measurement (Fig. 3). As the lattice period is close to the transversal-resolution limit of HCM, the

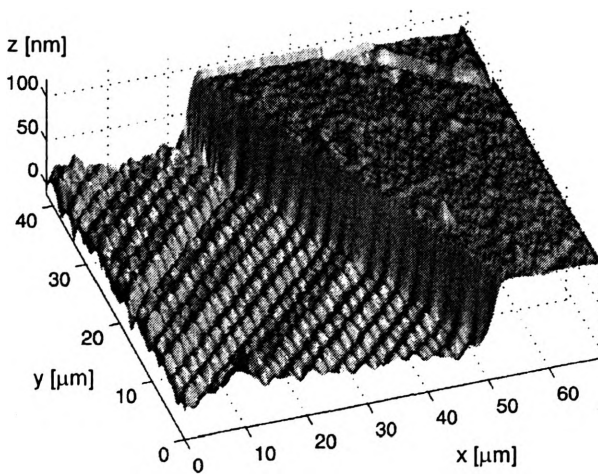


Fig. 2. Surface height profile of a specimen with a surface step. The profile was converted from the phase component of one optical section measured by HCM.

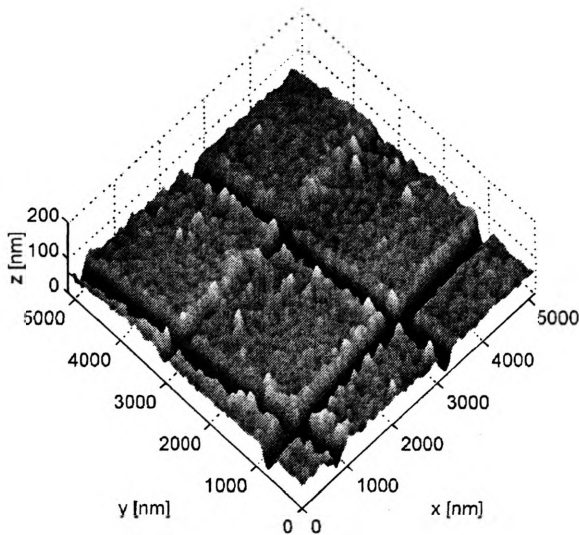


Fig. 3. Lattice structure in the deeper region of the surface in Fig. 2 observed by AFM.

shape of lattice elements is markedly deformed in the profile in Fig. 2. The measured height of the step is close to the reference value of about 60 nm obtained by Talystep, with differences of only several nanometers being detected. The r.m.s.-error estimate based on the values of $|a|$ is under 1 nm over the whole field except a few isolated points and the region of the very high height gradient. However, additional errors could be introduced by possible inaccuracy in the wavelength and angular-aperture determination and by the demonstrated influence of the transversal-resolution limit of the microscope on the image of fine surface details.

6. Multiple-optical-section measurement

The four-fold star shown in Fig. 4 was anisotropically etched to the depth of about $6\ \mu\text{m}$ in the surface of the Si plane substrate with the crystallographic orientation (100) covered by a nitride mask. The nitride mask was prepared by plasmochemical etching of nitride layer through the photoresist mask which was prepared by the electron lithography technique. Finally, the nitride mask was removed from Si substrate. The surface was measured by HCM in the same configuration as in Sec. 5, except the illumination which was provided by a halogen tungsten lamp with a narrow-band filter (the transmissivity maximum of FWHM = 15 nm is on the wavelength $\lambda = 547\ \text{nm}$).

The profile measurement was performed in two steps. First, the height maps of the lower (inner in Fig. 4) region and of the upper (outer) regions of the observed area of the specimen were measured separately by the procedure described in the previous section. During the measurement, the specimen was situated in the axial positions which correspond to intensity maxima in the two respective regions. The r.m.s.-errors under 1 nm for the lower region and under 2 nm for the upper region were estimated from the values of $|a|$. Areas with larger r.m.s.-error estimates than indicated were cut out from the resulting height map and they appear black in Fig. 4.

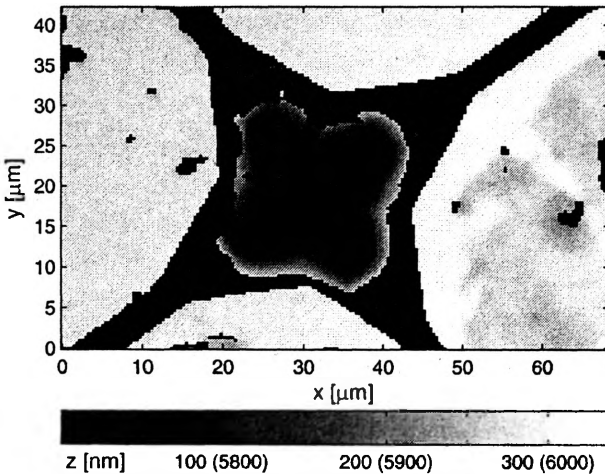


Fig. 4. Gray scale encoded surface height profile of a specimen with an etched four-fold star. The profile was converted from phase components of two optical sections. The height values for the upper (outer) regions are indicated in parenthesis.

In the second step, the two height maps were connected. The mean difference ($143 + m277.85$) nm between zero levels of the two maps was derived from the phase map corresponding to the lower region. The value of m was then determined by the independent measurement of the specimen axial displacement between the points of intensity maxima detection in the lower and upper regions. The necessary axial resolution was achieved by removing the narrow-band filter and thus switching to

broad-band illumination. The axial displacement was determined from the mean phase shift of all the observed image points considering the mean wavelength 508 nm of the broadband illumination. The value $m = 20$ and the corresponding height difference 5700 nm between the zero levels of the two maps were determined by this measurement. The measurement error estimate is under 25 nm, including possible inaccuracies in the determination of the wavelength and of the effective angular aperture. Figure 4 shows the resulting height map.

7. Conclusions

We have demonstrated that HCM can be effectively used for the high-precision profilometry of surfaces that can include even large and steep height steps. The high-precision measurement based on the phase imaging is complemented by a lower-precision but unambiguous measurement based on a depth-discriminated intensity imaging. The r.m.s.-error of the measurement caused by the noise can be estimated from the values of image amplitude modulus on the basis of calibration measurement. Additional errors can be caused by the limited transversal resolution of the microscope in the case of measurement of fine surface details. The systematic error possibly introduced by inaccuracy in determination of the wavelength and of the effective angular aperture can be prevented by a more precise determination of the proportionality constant between phase and height using a calibration sample with a surface step of a defined height.

Two-dimensional phase imaging of the surface is accessible almost in real time. It gives us the possibility to measure fast processes and, especially, to control precisely the sample position and tilt during the measurement without additional position detectors.

Acknowledgments – The specimens were prepared thanks to Mr. František Matějka, ISI CAS Brno, who performed also the Talystep measurement. The project is supported by the grant No. 101/00/0974 of the GA CR, by the grant CEZ:J22/98:262100002, and by the grant No. 1753/2002 of the University Development Fund of the MEYS CR.

References

- [1] AIGOUY L., DUBOIS A., BOCCARA A.C., *Near- and Farfield Measurements at Nanometer Scale*, [In] *Technical Digest of Focus on Microscopy 2000*, Shirahama 2000, p. 89.
- [2] WILSON T., *Confocal Microscopy*, [In] *Confocal Microscopy* [Ed.] T. Wilson, Academic Press, London 1990.
- [3] JORDAN H.J., WEGNER M., TIZIANI H., *Meas. Sci. Technol.* **9** (1998), 1142.
- [4] HAMILTON D.K., MATTHEWS H.J., *Optik* **71** (1985), 31.
- [5] CHMELÍK R., HARNA Z., *Opt. Eng.* **38** (1999), 1635.
- [6] INDEBETOUW G., KLYSUBUN P., *Opt. Lett.* **25** (2000), 212.

- [7] CHMELÍK R., *Correlation Microscopy, Alternative Method of Many-Channel Confocal Imaging*, Vutium, Brno 2002 (in Czech).
- [8] GOODMAN J.W., *Statistical Optics*, Wiley, New York 1985, p. 500.
- [9] CHMELÍK R., Proc. SPIE **4356** (2001), 118.

Received September 20, 2002